https://doi.org/10.3311/PPci.43302

Periodica Polytechnica Civil Engineering, 70(2), pp. 371–385, 2026

Finite Element Investigation of the Free Vibration Behavior of Functionally Graded Porous Timoshenko Beams on a Two-parameter Elastic Foundation with Shear Correction Effects

Mokhtar Dadouch[1,2*], Ismail Mechab[1,3], Noureddine Elmeiche[1,2], Belaïd Mechab[3]

[1] Department of Civil Engineering and Public Works, Faculty of Technology, Djillali Liabès University, 22000 Sidi Bel Abbès, P.O.B. 89, Algeria
[2] Laboratory of Civil Engineering and Environment, Djillali Liabès University, 22000 Sidi Bel Abbès, P.O.B. 89, Algeria
[3] Laboratory of Mechanics and Physics of Materials (LMPM), Djillali Liabès University, 22000 Sidi Bel Abbès, P.O.B. 89, Algeria
[*] Corresponding author, e-mail: mokhtar.dadouch@dl.univ-sba.dz

Received: 09 January 2026, Accepted: 31 March 2026, Published online: 09 April 2026

Abstract

This study investigates the free vibration behavior of porous functionally graded beams using Timoshenko theory on a Winkler–Pasternak foundation. Such beams are commonly used in practical engineering applications, including aerospace structures and civil engineering components, where vibration control and weight efficiency are critical. The main advantage of the proposed method lies in its ability to capture the coupled effects of porosity and material gradation on transverse shear behavior, which are neglected in classical models using constant shear factors. The effects of key parameters are analyzed, including the material gradation index material, the foundation coefficients, porosity distributions, and transverse shear deformation through an adjusted correction factor. The governing equations of motion are derived using Hamilton's principle. The formulation is generally applicable to different boundary conditions, material configurations, and elastic foundation parameters. The proposed model is validated through comparisons with results from the literature, demonstrating agreement and confirming its reliability. The numerical results indicate that increasing the gradation index materials leads to a reduction in natural frequencies due to decreased material stiffness, an effect that becomes more pronounced for higher vibration modes. Conversely, the combined influence of the foundation parameters results in an increase in natural frequencies, highlighting the stiffening effect of the foundation. The shear correction factor decreases with increasing index material. Finally, comparing the natural frequencies obtained using a shear correction factor for isotropic materials with those of corrected porous FGM materials highlights the need to include coupled porosity–gradation effects in the dynamic analysis of FGM beams.

Keywords

FGM beam, Timoshenko beam, porosity, corrective shear factor, elastic deposition, finite element method

1 Introduction

Functional gradient materials (FGMs) have emerged as an innovative solution for enhancing the performance of structures in severe environments by smoothly combining the characteristics of two or more constituent materials [1, 2].

This continuous variation in properties, often described by a power-law distribution, reduces stress concentrations and improves resistance to thermal and mechanical shocks, making FGMs highly attractive for aeronautical, space, and biomedical applications [3]. However, realistic manufacturing processes-such as plasma sintering or sputtering-inevitably introduce porosity, adding heterogeneities that may degrade stiffness and adversely affect the dynamic behavior of FGM structures [4].

In structural design, understanding the vibrational response of beams is crucial, particularly in avoiding resonance phenomena that can lead to premature failure [5]. Timoshenko beam theory, which incorporates both shear deformation and rotary inertia, provides a critical refinement of the classical Euler–Bernoulli theory, especially for short beams or structures subjected to high-frequency excitation [6]. Extending this theory to porous FGM beams enables a more accurate representation of their mechanical

Cite this article as: Dadouch, M., Mechab, I., Elmeiche, N., Mechab, B. "Finite Element Investigation of the Free Vibration Behavior of Functionally Graded Porous Timoshenko Beams on a Two-parameter Elastic Foundation with Shear Correction Effects", Periodica Polytechnica Civil Engineering, 70(2), pp. 371–385, 2026. https://doi.org/10.3311/PPci.43302

behavior by capturing the combined effects of continuously varying material properties and porosity-induced defects.

Porosity significantly alters the elastic modulus, density, and stiffness of FGMs, and must therefore be explicitly considered in free vibration analyses [7]. Various porosity distributions-such as symmetric, asymmetric, or gradient-dependent configurations-have been introduced to reflect real manufacturing conditions or meet design optimization requirements [8–11]. Numerous studies have shown that increasing porosity content leads to a marked reduction in natural frequencies, thereby influencing the dynamic performance and stability of the structure [12–15].

Support conditions also play a decisive role in the dynamic behavior of beams. To more realistically model the interaction between a beam and its supporting medium, two-parameter foundation models combining Winkler and Pasternak components are commonly used [16–19]. The Winkler model assumes that the foundation reaction is proportional to the local displacement. At the same time, the Pasternak component incorporates a shear interaction term that couples neighboring displacements, thereby providing a more realistic representation of semi-infinite or composite foundations [20]. In dynamic analyses, these parameters directly influence natural frequencies and mode shapes, making their inclusion essential for accurate structural predictions [21].

Given the complexity of the coupled phenomena governing porous FGM beams resting on two-parameter foundations – particularly in dynamic contexts – efficient numerical approaches are required. The finite element method (FEM) provides a powerful and flexible framework that can accommodate spatially varying material properties, porosity effects, boundary conditions, and foundation–structure interactions [22]. Additionally, FEM is well-suited for large-scale problems, providing accurate solutions for complex geometries and heterogeneous material distributions [23].

Hamzi et al. [6] and Drici et al. [19] examined the influence of functional grading on the natural frequencies of non-porous beams or plates, demonstrating that dynamic responses are susceptible to gradient indices and constituent distributions. However, relatively few studies have simultaneously addressed the combined effects of porosity, complex elastic foundations, and functional grading within a dynamic framework, particularly for thick Timoshenko beams [24, 25].

In this context, the shear correction factor is particularly important. Widely used in structural mechanics to adjust shear stiffness predictions, it compensates for the simplified representation of non-uniform shear stress distributions inherent in beam and plate theories [19, 26–28]. Classical formulations, such as $k = 5/6$, may lead to inaccuracies when applied to porous FGMs, where heterogeneity has a strong influence on shear behavior. Recent studies propose porosity- and gradient-dependent shear correction formulations to improve the accuracy of static and dynamic responses.

A broad range of recent advances further highlights the importance of accurately modelling complex material behaviors and dynamic interactions. Zou et al. [29] developed a versatile device that generates customizable nonlinear restoring forces for improved vibration isolation and energy harvesting. Zhang et al. [30] investigated damped vibration in GPL-reinforced magnetorheological elastomer panels using a hybrid GDQ formulation. Tang et al. [31] proposed a coupled model for intelligent compaction integrating roller dynamics and layered poroelastic subgrades. Deng and Gao [32] introduced a curved acoustic black hole absorber achieving broadband vibroacoustic attenuation. Wei et al. [33] examined steel tube-confined UHPC columns, demonstrating enhanced strength and ductility. Dai et al. [34] developed a multiple TMD-inerter configuration to mitigate vortex-induced vibrations in flexible bridges. Zhou et al. [35] formulated a scaled nonlocal integral model achieving mesh- and length-independent softening predictions. Long et al. [36] proposed a multiscale FE framework for progressive collapse analysis in RC assemblies. Ma et al. [37] linked snow's macroscopic compression to the microstructural breakage of ice bonds. Lu et al. [38] developed an elastoplastic concrete model including strain rate as a constitutive variable. Dhuria et al. [39] analyzed the effect of porosity distribution on FG porous plates using IHSDT. Srikarun et al. [40] investigated linear and nonlinear bending of FG porous sandwich beams. Tran et al. [41] applied a smoothed MITC3 element to FG porous variable-thickness plates. Kiarasi et al. [42] reviewed FG porous structures reinforced with graphene platelets, highlighting their micromechanical modelling and multifunctional potential.

Given these findings, the present work aims to analyze the free vibration response of a Timoshenko beam made of porous functional gradient material resting on a two-parameter elastic foundation, using a finite element approach. Such beams are commonly used in practical engineering applications, including aerospace structures, MEMS, and civil engineering components, where vibration control and weight efficiency are critical. The main advantage of the proposed method lies in its ability to capture the coupled effects of porosity and material gradation on transverse shear behavior, which are neglected in classical

models using constant shear factors. The primary objective is to evaluate the combined influence of the gradient index, porosity distributions (Types I, II, and III), and the Winkler and Pasternak foundation parameters, as well as boundary conditions, on the natural frequencies of the system. The formulation is generally applicable to different boundary conditions, material configurations, and elastic foundation parameters. Particular emphasis is placed on comparing natural frequencies obtained using a porosity-corrected shear factor with those computed using the classical factor, in order to quantify the relevance of this correction for accurate dynamic analysis. Incorporating a shear correction factor that accounts for porosity-and the resultant variation of material properties-significantly influences the vibrational response. This highlights that the assumed anisotropy in material modelling constitutes a key parameter in the analysis. The proposed correction prevents the overestimation of stiffness inherent in classical formulations, thereby ensuring more reliable safety margins for critical engineering applications.

2 Development of the theory

Fig. 1 shows the displacement field based on the theory of first-order shear deformation, which may be expressed as:

$$\begin{cases} U(x,z) = u(x) + z\phi(x) \\ W(x,z) = w(x) \end{cases}. \tag{1}$$

The fundamental assumptions employed for developing the equations of motion for free vibration are as follows:

1. The beam studied, based on Timoshenko theory, assumes that plane cross-sections remain plane after deformation, but are not necessarily perpendicular to the neutral axis, thus accounting for the effects of transverse shear deformation and rotatory inertia.
2. This assumption accounts for the effect of transverse shear (*via* the shear correction factor) and the effect of rotatory inertia. It is essential for the study of short and thick beams (or FGM beams whose shear rigidity varies, as mentioned in your previous summary).
3. Elastic behavior: the entire FGM beam is assumed to exhibit linear elastic behavior.
4. Small deformations: displacements, rotations, and strains are assumed to be small relative to the beam's thickness.
5. Anisotropic layers: each infinitesimal layer across the beam's thickness is modelled as an anisotropic layer.
6. Property grading: the Young's modulus and the Poisson's ratio vary continuously and exclusively in the thickness direction, governed by the variation in porosity.
7. Elastic foundation: the beam is supported by an elastic foundation of the Winkler-Pasternak type.
8. Shear correction factor: the shear correction factor for the porous FGM beam is not equal to that of an isotropic prismatic material (k = 5/6).
9. Factor dependency: the shear correction factor is dependent upon both the anisotropy and the porosity of the beam material.

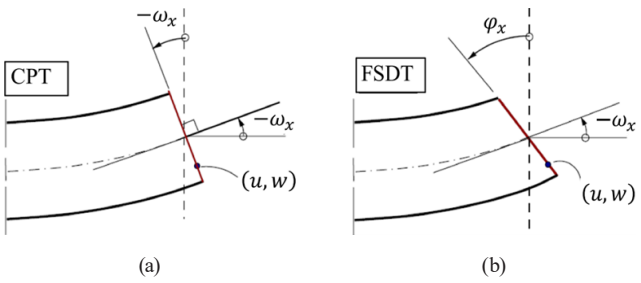

Fig. 1 Displacement field based on the theory used as the basis for the analysis: (a) Euler-Bernoulli hypothesis; (b) Timoshenko hypothesis

Let us consider a porous FGM beam of length L, width b and height h, as shown in Fig. 2 is graduated from metal at the bottom and ceramic at the top; the beam properties (such as Young's modules $E(z)$, density $\rho(z)$ and the poisson coefficient) are assumed to be varied according to its height in accordance with the power law distribution with the distribution of porosity across the thickness [11, 39–41]:

$$\begin{aligned} E(z) &= \left[(E_t - E_b)\left(\frac{z}{h}+\frac{1}{2}\right)^p + E_b\right]\left(1 - e_0\psi(z)\right) \\ \rho(z) &= \left[(\rho_t - \rho_b)\left(\frac{z}{h}+\frac{1}{2}\right)^p + \rho_b\right]\left(1 - e_b\psi(z)\right), \\ \nu(z) &= \left[(\nu_t - \nu_b)\left(\frac{z}{h}+\frac{1}{2}\right)^p + \nu_b\right]\left(1 - e_0\psi(z)\right) \end{aligned} \tag{2}$$

where e_0 is the coefficient of porosity applied to the Young modulus, $E(z)$ is Young's modulus, $G(z)$ is the shear coefficient, e_m is the coefficient of porosity applied to the density $\rho(z)$, such that $0 < (e_0, e_b) < 1$.

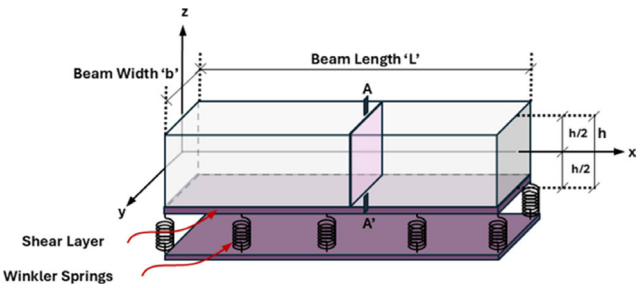

Fig. 2 Configuration of the FG beam studied in this work

The porosity coefficient e_0 is written [11, 42]:

$$\begin{aligned} e_0 &= 1-\frac{E(z)}{E^*(z)} \\ e_b &= 1-\frac{\rho(z)}{\rho^*(z)} \end{aligned}. \tag{3}$$

The relative Young's modulus shows in Eq. (4) [11, 42]:

$$\frac{E(z)}{E^*(z)} = \left(\frac{\rho(z)}{\rho^*(z)}\right)^2. \tag{4}$$

From Eqs. (3) and (4), one can find the relationship that connects the coefficient e_0 and e_b:

$$\sqrt{1-e_0\psi(z)} = 1-e_b\psi(z). \tag{5}$$

The expression of e_b as a function of e_0 and $\psi(z)$:

$$e_b = \frac{h-\int_{\frac{-h}{2}}^{\frac{h}{2}}\sqrt{1-e_0\psi(z)}dz}{\int_{\frac{-h}{2}}^{\frac{h}{2}}\psi(z)dz}. \tag{6}$$

With $\psi(z)$ is a distribution of porosity that presents the following three types can be seen in Fig. 3 [11, 39–41]:

$$\begin{aligned} &\text{Type I } (\text{center enhanced}) \ \psi(z) = \cos\left(\frac{\pi z}{h}\right) \\ &\text{Type II } (\text{top enhanced}) \ \psi(z) = \cos\left[\frac{\pi}{2}\left(\frac{z}{h}+\frac{1}{2}\right)\right] \\ &\text{Type III } (\text{bottom enhanced}) \ \psi(z) = \cos\left[\frac{\pi}{2}\left(\frac{z}{h}-\frac{1}{2}\right)\right] \end{aligned}. \tag{7}$$

Three types of porosity distributions across the thickness of the functionally graded material (FGM) beam are illustrated in Fig. 3. The first distribution corresponds to a concentration of porosity at the mid-plane of the beam, the second shows a concentration of porosity in the lower region. At the same time, the third exhibits a localized concentration in the upper region of the beam. In Fig. 3 $E(z)$ and $\rho(z)$ represent the minimum values of Young's modulus, shear modulus, and mass density of the porous metal, respectively.

Similarly, $E^*(z)$ and $\rho^*(z)$ denote the maximum values of the same parameters.

In the static case, for the analysis of plate bending, the equilibrium equation for the stresses acting in the x-z plane in the absence of body forces is:

$$\frac{\partial\sigma_{xx}}{\partial x}+\frac{\partial\tau_{xz}}{\partial z}=0, \tag{8}$$

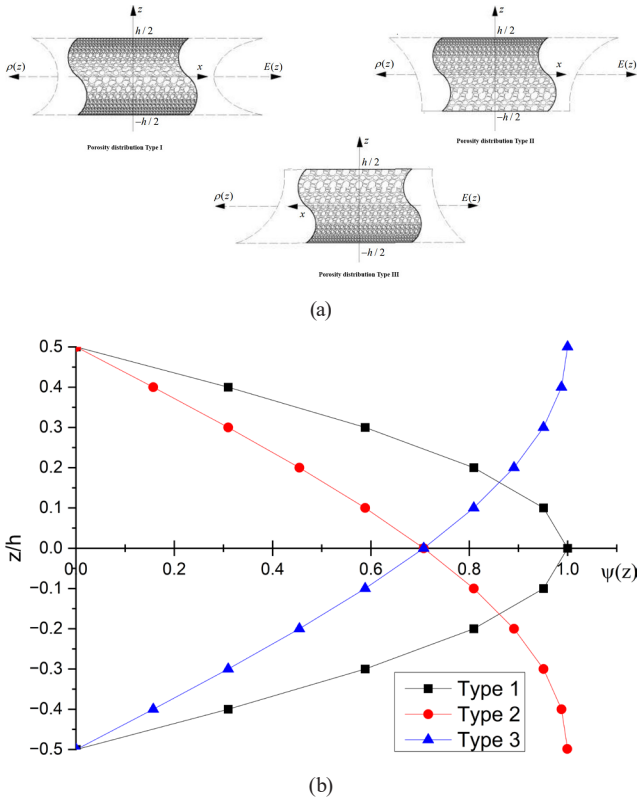

Fig. 3 Porosity distributions: (a) geometric representations through the beam thickness; (b) porosity distribution functions through the beam thickness

and

$$\begin{Bmatrix}\sigma_{xx}\\ \tau_{xz}\end{Bmatrix} = \begin{bmatrix}Q_{11}(z) & 0\\ 0 & Q_{55}(z)\end{bmatrix}\begin{Bmatrix}\varepsilon_{xx}\\ \gamma_{xz}\end{Bmatrix}, \tag{9}$$

where the rigidities $Q_{ij}(z)$ depend on the Young's modulus E and the Poisson coefficient.

The deformation field can be expressed as follows:

$$\begin{aligned} \varepsilon_{xx} &= \frac{\partial u}{\partial x}+z\frac{\partial\phi}{\partial x} \\ \gamma_{xz} &= w+\frac{\partial\phi}{\partial x} \end{aligned}. \tag{10}$$

The following connection between forces, deformations, and curvatures results from the limitations, as stated in Eq. (9), through the thickness of the beam:

$$\begin{Bmatrix}N\\ M\end{Bmatrix} = \iint\sigma_{xx}\begin{Bmatrix}1\\ z\end{Bmatrix}dS = \begin{bmatrix}A_{11} & B_{11}\\ B_{11} & D_{11}\end{bmatrix}\begin{Bmatrix}\frac{\partial u}{\partial x}\\ \frac{\partial\phi}{\partial x}\end{Bmatrix}. \tag{11}$$

The following are expressions for rigidities:

$$\left\{A_{11}, B_{11}, D_{11}\right\} = \int_{-\frac{h}{2}}^{\frac{h}{2}} \frac{E(z)}{1-\nu^2}\left\{1, z, z^2\right\} dz, \tag{12}$$

$$\tau_{xz} = \frac{E(z)}{2\left(1+\nu(z)\right)}\gamma_{xz}. \tag{13}$$

Inverting the complete stiffness matrix in Eq. (11) yields:

$$\begin{Bmatrix} \frac{\partial u}{\partial x} \\ \frac{\partial \phi}{\partial x} \end{Bmatrix} = \begin{bmatrix} \frac{D_{11}}{A_{11}D_{11} - B_{11}^2} & -\frac{B_{11}}{A_{11}D_{11} - B_{11}^2} \\ -\frac{B_{11}}{A_{11}D_{11} - B_{11}^2} & \frac{A_{11}}{A_{11}D_{11} - B_{11}^2} \end{bmatrix} \begin{Bmatrix} N \\ M \end{Bmatrix}. \tag{14}$$

The transverse shear stress (τ_{xz}) is integrated throughout the height of the FGM beam to determine the shear stress relationship, which yields the following result:

$$Q_{xz} = \kappa \int_{-\frac{h}{2}}^{\frac{h}{2}} \frac{E(z)}{2\left(1+\nu(z)\right)} dz\gamma_{xz} = \kappa A_{55}^s \gamma_{xz}, \tag{15}$$

where κ is the shear factor.

The following form represents the fundamental equations of a beam with the first-order shear displacement field in FGM:

$$\begin{Bmatrix} \frac{\partial u}{\partial x} \\ \frac{\partial \phi}{\partial x} \\ \phi + \frac{\partial w}{\partial x} \end{Bmatrix} = \begin{bmatrix} \frac{D_{11}}{A_{11}D_{11} - B_{11}^2} & -\frac{B_{11}}{A_{11}D_{11} - B_{11}^2} & 0 \\ -\frac{B_{11}}{A_{11}D_{11} - B_{11}^2} & \frac{A_{11}}{A_{11}D_{11} - B_{11}^2} & 0 \\ 0 & 0 & \frac{1}{\kappa A_{55}^s} \end{bmatrix} \begin{Bmatrix} N \\ M \\ Q_{xz} \end{Bmatrix}. \tag{16}$$

By incorporating the stress equilibrium Eq. (8), the expression for shear stress is given as follows:

$$\tau_{xz} = -\int_{-\frac{h}{2}}^{z} \frac{\partial \sigma_{xx}}{\partial x} = -\int_{-\frac{h}{2}}^{z} Q_{11}(z)\left(\frac{\partial u}{\partial x} + z\frac{\partial \phi}{\partial x}\right)_{,x} dz. \tag{17}$$

By substituting the expression for $\partial u/\partial x$ and $\partial \phi/\partial x$ from Eq. (16) into τ_{xz}, we obtain:

$$\begin{aligned} \tau_{xz} = &-\int_{-\frac{h}{2}}^{z} \frac{\partial N}{\partial x}\begin{pmatrix} Q_{11}(z)\frac{D_{11}}{A_{11}D_{11} - B_{11}^2} \\ -zQ_{11}(z)\frac{B_{11}}{A_{11}D_{11} - B_{11}^2} \end{pmatrix} \\ &+\frac{\partial M}{\partial x}\begin{pmatrix} -Q_{11}(z)\frac{B_{11}}{A_{11}D_{11} - B_{11}^2} \\ +zQ_{11}(z)\frac{A_{11}}{A_{11}D_{11} - B_{11}^2} \end{pmatrix} dz. \end{aligned} \tag{18}$$

We have $\partial N/\partial x = 0$ and $\partial M/\partial x = Q_{xz}$, the shear stress Eq. (15) becomes:

$$\tau_{xz} = -\int_{-\frac{h}{2}}^{z} Q_{xz}\begin{pmatrix} -Q_{11}(z)\frac{B_{11}}{A_{11}D_{11} - B_{11}^2} \\ +zQ_{11}(z)\frac{A_{11}}{A_{11}D_{11} - B_{11}^2} \end{pmatrix} dz. \tag{19}$$

Equation (20) gives the total deformation energy U of the FGM beam:

$$\begin{aligned} U &= \frac{1}{2}\int_{-\frac{h}{2}}^{\frac{h}{2}} \frac{\tau_{xz}^2}{Q_{55}(z)} dz \\ &= \frac{1}{2}\int_{-\frac{h}{2}}^{\frac{h}{2}} \frac{\left(\int_{-\frac{h}{2}}^{z} Q_{xz}\begin{pmatrix} -Q_{11}(z)\frac{B_{11}}{A_{11}D_{11} - B_{11}^2} \\ +zQ_{11}(z)\frac{A_{11}}{A_{11}D_{11} - B_{11}^2} \end{pmatrix} dz\right)^2}{Q_{55}(z)} dz, \end{aligned} \tag{20}$$

The constitutive relationship $Q_{xz} = \kappa A_{55}^s \gamma_{xz}$, the constant transverse shear deformation, is as follows:

$$U = \frac{1}{2}\frac{Q_{xy}^2}{\kappa A_{55}^s}. \tag{21}$$

The shear correction factor is given by:

$$\begin{aligned} &\frac{1}{2}\frac{{Q_{xz}}^2}{\kappa A_{55}^s} \\ &= \frac{1}{2}\int_{-\frac{h}{2}}^{\frac{h}{2}} \frac{\left(\int_{-\frac{h}{2}}^{z} Q_{xz}\begin{pmatrix} -Q_{11}(z)\frac{B_{11}}{A_{11}D_{11} - B_{11}^2} \\ +zQ_{11}(z)\frac{A_{11}}{A_{11}D_{11} - B_{11}^2} \end{pmatrix} dz\right)^2}{Q_{55}(z)} dz, \end{aligned} \tag{22}$$

$$\kappa = \frac{1}{A_{55}^{s}\int_{-\frac{h}{2}}^{\frac{h}{2}} \frac{\left(\int_{-\frac{h}{2}}^{z}\begin{pmatrix} -Q_{11}(z)\dfrac{B_{11}}{A_{11}D_{11}-B_{11}^{2}} \\ +zQ_{11}(z)\dfrac{A_{11}}{A_{11}D_{11}-B_{11}^{2}}\end{pmatrix}dz\right)^{2}}{Q_{55}(z)}dz}. \tag{23}$$

2.1 Free vibration of beams in FGM

The strain energy of a beam of length L with a cross-sectional area denoted by A can be defined from the volumetric integral:

$$W_{int} = \iiint \left(\sigma_{xx}\varepsilon_{xx} + \tau_{xz}\gamma_{xz}\right) dA dx. \tag{24}$$

The energy function can be written in matrix form as:

$$W_{int} = \iiint \left(\begin{Bmatrix} u' & \phi' & w'+\phi \end{Bmatrix} \begin{bmatrix} A_{11} & B_{11} & 0 \\ B_{11} & D_{11} & 0 \\ 0 & 0 & A_{55}^{s} \end{bmatrix} \begin{Bmatrix} u' \\ \phi' \\ w'+\phi \end{Bmatrix} \right) dA dx. \tag{25}$$

The variation of the internal energy functional Eq. (24) leads to the variational equality of the model as a function of internal forces:

$$W_{int} = \iiint \left(Nu' + M\phi' + Q_{xz}\gamma_{xz}\right) dx, \tag{26}$$

with

$$\begin{Bmatrix} N \\ M \\ Q_{xz} \end{Bmatrix} = \begin{bmatrix} A_{11} & B_{11} & 0 \\ B_{11} & D_{11} & 0 \\ 0 & 0 & A_{55}^{s} \end{bmatrix} \begin{Bmatrix} u' \\ \phi' \\ w'+\phi \end{Bmatrix}, \tag{27}$$

where N, M and Q_{xz} are, respectively, the normal force, bending moment, and the shear stress.

The total kinetic energy of the beam in FGM can be written as:

$$T = \iiint \rho(z)\left(\dot{U}^{2} + \dot{W}^{2}\right) dA dx, \tag{28}$$

where $\rho(z)$ is the density per unit volume. The upper dot represents the derivative with respect to time t.

In Eq. (29) f_e is the reaction force density of the foundation, k_w and k_p are the foundation parameters, respectively:

$$f_e = k_w w - k_p \frac{\partial^2 w}{\partial x^2}. \tag{29}$$

The deformation behavior of the elastic foundation is:

$$W_{f_e} = \frac{1}{2}\iint \left(k_w w^2 + k_p \left(\frac{\partial w}{\partial x}\right)^2 \right) dS. \tag{30}$$

The equilibrium equations and associated boundary conditions for FGM beams will be derived using Hamilton's principle, which can be stated in this form:

$$\int_{t_1}^{t_2} \left(W_{int} + W_{f_e} - T\right) dt = 0. \tag{31}$$

The equilibrium equations are obtained from Eq. (31) by integrating displacement gradients by parts and setting the coefficients ∂u, ∂w, $\partial \phi$ independently to zero:

$$\frac{\partial N}{\partial x} = I_1 \frac{\partial^2 u}{\partial t^2} + I_2 \frac{\partial^2 \phi}{\partial t^2}, \tag{32}$$

$$\frac{\partial M}{\partial x} - Q_{xz} = I_2 \frac{\partial^2 u}{\partial t^2} + I_3 \frac{\partial^2 \phi}{\partial t^2}, \tag{33}$$

$$\frac{\partial V}{\partial x} - f_e = I_1 \frac{\partial^2 w_0}{\partial t^2}, \tag{34}$$

$$\{I_1, I_2, I_3\} = \int_{-\frac{h}{2}}^{\frac{h}{2}} \rho(z)\{1, z, z^2\} dz. \tag{35}$$

The interpolation functions of the displacement field in the finite element formulation are derived by solving a system of ordinary differential equations, corresponding to the static component of the governing differential equations defined in Eqs. (32) to (34):

$$\phi(x) = \frac{1}{2}C_4 x^2 + C_5 x + C_6, \tag{36}$$

$$u(x) = \frac{1}{2}\frac{B_{11}}{A_{11}}C_1 x^2 - \frac{B_{11}C_5 - A_{11}C_1}{A_{11}}x - \frac{B_{11}C_6 - A_{11}C_2}{A_{11}}, \tag{37}$$

$$w(x) = \frac{1}{6}C_4 x^3 - \frac{1}{2}C_5 x^3 - \left(\frac{1}{6}\frac{B_{11}^2 - A_{11}D_{11}}{A_{55}^{s}A_{11}}C_4 + C_6\right)x + C_3. \tag{38}$$

The constants C_1, C_2, C_3, C_4, C_5, C_6, a_7 are obtained according to the degrees of freedom illustrated in Fig. 4:

$$\begin{cases} u(0) = u_1 \\ w(0) = w_1 \\ \phi(0) = \phi_1 \end{cases} \text{ and } \begin{cases} u(L_e) = u_2 \\ w(L_e) = w_2 \\ \phi(L_e) = \phi_2 \end{cases}. \tag{39}$$

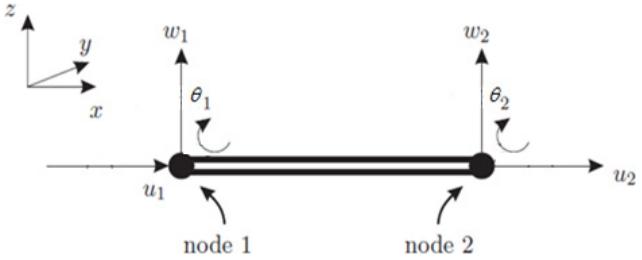

Fig. 4 Discretization of the beam length

After calculating the displacement constants $u(x)$, $w(x)$ and $\phi(x)$, shall be written as follows:

$$C_1 = -\frac{u_1}{L_e} - \frac{B_{11}\theta_1}{L_e A_{11}} + \frac{u_2}{L_e} + \frac{B_{11}\theta_2}{L_e A_{11}}, \tag{40}$$

$$C_2 = \frac{B_{11}\theta_1}{A_{11}} + u_1, \tag{41}$$

$$C_3 = w_1, \tag{42}$$

$$C_{4,1} = -\frac{12A_{55}^s A_{11} w_1}{L_e\left(A_{11}A_{55}^s L_e^2 + 12A_{11}D_{11} - 12B_{11}^2\right)}, \tag{43}$$

$$C_{4,2} = \frac{6A_{55}^s A_{11}\theta_1}{A_{11}A_{55}^s L_e^2 + 12A_{11}D_{11} - 12B_{11}^2}, \tag{44}$$

$$C_{4,3} = \frac{12A_{55}^s A_{11} w_2}{L_e\left(A_{11}A_{55}^s L_e^2 + 12A_{11}D_{11} - 12B_{11}^2\right)}, \tag{45}$$

$$C_{4,4} = \frac{6A_{55}^s A_{11}\theta_2}{A_{11}A_{55}^s L_e^2 + 12A_{11}D_{11} - 12B_{11}^2}, \tag{46}$$

$$C_4 = C_{4,1} + C_{4,2} + C_{4,3} + C_{4,4}, \tag{47}$$

$$C_{5,1} = \frac{6A_{55}^s A_{11} w_1}{A_{11}A_{55}^s L_e^2 + 12A_{11}D_{11} - 12B_{11}^2}, \tag{48}$$

$$C_{5,2} = \frac{2\left(2A_{11}A_{55}^s L_e^2 + 6A_{11}D_{11} - 6B_{11}^2\right)\theta_1}{L_e\left(A_{11}A_{55}^s L_e^2 + 12A_{11}D_{11} - 12B_{11}^2\right)}, \tag{49}$$

$$C_{5,3} = \frac{6A_{55}^s A_{11} w_2}{A_{11}A_{55}^s L_e^2 + 12A_{11}D_{11} - 12B_{11}^2}, \tag{50}$$

$$C_{5,4} = \frac{2\left(A_{11}A_{55}^s L_e^2 - 6A_{11}D_{11} + 6B_{11}^2\right)\theta_2}{L_e\left(A_{11}A_{55}^s L_e^2 + 12A_{11}D_{11} - 12B_{11}^2\right)}, \tag{51}$$

$$C_5 = C_{5,1} - C_{5,2} - C_{5,3} - C_{5,4}, \tag{52}$$

$$C_6 = \theta_1. \tag{53}$$

We put:

$$e_1 = \frac{B_{11}}{A_{11}},\ e_2 = A_{11}A_{55}^s,\ e_3 = A_{11}D_{11} - B_{11}^2. \tag{54}$$

The six constants become:

$$C_6 = \theta_1, \tag{55}$$

$$C_4 = \frac{6e_2\theta_2}{L_e^2 e_2 + 12e_3} + \frac{6e_2\theta_1}{L_e^2 e_2 + 12e_3} - \frac{12e_2 w_1}{L_e\left(L_e^2 e_2 + 12e_3\right)} + \frac{12e_2 w_2}{L_e\left(L_e^2 e_2 + 12e_3\right)}, \tag{56}$$

$$C_1 = -\frac{u_1}{L_e} + \frac{u_2}{L_e} + \frac{e_1\theta_2}{L_e} - \frac{e_1\theta_1}{L_e}, \tag{57}$$

$$C_2 = e_1\theta_1 + u_1, \tag{58}$$

$$C_3 = w_1, \tag{59}$$

$$C_{5,1} = -\frac{2L_e e_2\theta_2}{L_e^2 e_2 + 12e_3} - \frac{4L_e e_2\theta_1}{L_e^2 e_2 + 12e_3} + \frac{6w_1 e_2}{L_e^2 e_2 + 12e_3}, \tag{60}$$

$$C_{5,2} = \frac{6w_2 e_2}{L_e^2 e_2 + 12e_3} - \frac{12\theta_1 e_3}{L_e\left(L_e^2 e_2 + 12e_3\right)} + \frac{12\theta_2 e_3}{L_e\left(L_e^2 e_2 + 12e_3\right)}, \tag{61}$$

$$C_5 = C_{5,1} - C_{5,2}. \tag{62}$$

By substituting the six constants in the displacement terms $u(x)$, $w(x)$ and $\phi(x)$, will be written as follows:

$$u(x)_1 = \left(-\frac{x}{L_e} + 1\right)u_1 + \left(\frac{6e_1e_2x^2}{L_e\left(L_e^2e_2 + 12e_3\right)} - \frac{6e_1e_2x}{L_e^2e_2 + 12e_3}\right)w_1, \tag{63}$$

$$u(x)_2 = \left(-\frac{3e_1e_2x^2}{L_e^2e_2 + 12e_3} - \left(e_1\begin{pmatrix}-\frac{4L_ee_2}{L_e^2e_2 + 12e_3}\\ -\frac{12e_3}{L_e\left(L_e^2e_2 + 12e_3\right)}\end{pmatrix} + \frac{e_1}{L_e}\right)x\right)\theta_1, \tag{64}$$

$$u(x)_3 = \frac{xu_2}{L_e} + \left(-\frac{6e_1e_2x^2}{L_e\left(L_e^2e_2 + 12e_3\right)} + \frac{6e_1e_2x}{L_e^2e_2 + 12e_3}\right)w_2, \tag{65}$$

$$u(x)_4 = \left(-\frac{3e_1e_2x^2}{L_e^2e_2 + 12e_3} - \left(e_1\begin{pmatrix}-\frac{2L_ee_2}{L_e^2e_2 + 12e_3}\\ +\frac{12e_3}{L_e\left(L_e^2e_2 + 12e_3\right)}\end{pmatrix} - \frac{e_1}{L_e}\right)x\right)\theta_2, \tag{66}$$

$$u(x) = u(x)_1 + u(x)_2 + u(x)_3 + u(x)_4, \tag{67}$$

$$w(x)_1 = \begin{pmatrix}\frac{2e_2x^3}{L_e\left(L_e^2e_2 + 12e_3\right)} - \frac{3e_2x^2}{L_e^2e_2 + 12e_3}\\ -\frac{12e_3x}{L_e\left(L_e^2e_2 + 12e_3\right)} + 1\end{pmatrix}w_1, \tag{68}$$

$$w(x)_2 = \left(-\frac{e_2x^3}{L_e^2e_2 + 12e_3} - \frac{1}{2}\left(-\frac{4L_ee_2}{L_e^2e_2 + 12e_3} - \frac{12e_3}{L_e\left(L_e^2e_2 + 12e_3\right)}\right)\right)x^2 - \frac{1}{6}xe_2\left(\frac{6}{2}e_2 - \frac{36e_3e_2}{L_e^2e_2 + 12e_3}\right)\theta_1, \tag{69}$$

$$w(x)_3 = \left(-\frac{2e_2x^3}{L_e\left(L_e^2e_2+12e_3\right)} + \frac{3e_2x^2}{L_e^2e_2+12e_3} + \frac{12e_3x}{L_e\left(L_e^2e_2+12e_3\right)} \right) w_2, \tag{70}$$

$$w(x)_4 = \left(-\frac{e_2x^3}{L_e^2e_2+12e_3} - \frac{1}{2}\left(-\frac{2L_ee_2}{L_e^2e_2+12e_3} + \frac{12e_3}{L_e\left(L_e^2e_2+12e_3\right)} \right) x^2 + \frac{6e_3x}{L_e^2e_2+12e_3} \right) \theta_2, \tag{71}$$

$$w(x) = w(x)_1 + w(x)_2 + w(x)_3 + w(x)_4, \tag{72}$$

$$\phi(x)_1 = \left(-\frac{6e_2x^2}{L_e\left(L_e^2e_2+12e_3\right)} + \frac{6e_2x}{L_e^2e_2+12e_3} \right) w_1, \tag{73}$$

$$\phi(x)_2 = \left(\frac{3e_2x^2}{L_e^2e_2+12e_3} + \left(-\frac{4L_ee_2}{L_e^2e_2+12e_3} - \frac{12e_3}{L_e\left(L_e^2e_2+12e_3\right)} \right) x + 1 \right) \theta_1, \tag{74}$$

$$\phi(x)_3 = \left(\frac{6e_2x^2}{L_e\left(L_e^2e_2+12e_3\right)} - \frac{6e_2x}{L_e^2e_2+12e_3} \right) w_2, \tag{75}$$

$$\phi(x)_4 = \left(\frac{3e_2x^2}{L_e^2e_2+12e_3} + \left(-\frac{2L_ee_2}{L_e^2e_2+12e_3} + \frac{12e_3}{L_e\left(L_e^2e_2+12e_3\right)} \right) x \right) \theta_2, \tag{76}$$

$$\phi(x) = \phi(x)_1 + \phi(x)_2 + \phi(x)_3 + \phi(x)_4. \tag{77}$$

The displacements in Eqs. (68), (73) and (78) can be written in the following matrix form:

$$\{u, w, \phi\} = \begin{bmatrix} N_1(x) & N_2(x) & N_3(x) & N_4(x) & N_5(x) & N_6(x) \\ N_7(x) & N_8(x) & N_9(x) & N_{10}(x) & N_{11}(x) & N_{12}(x) \\ N_{13}(x) & N_{14}(x) & N_{15}(x) & N_{16}(x) & N_{17}(x) & N_{18}(x) \end{bmatrix} \times \begin{Bmatrix} u_1 \\ w_1 \\ \theta_1 \\ u_2 \\ w_2 \\ \theta_2 \end{Bmatrix}. \tag{78}$$

Substituting Eqs. (68), (73) and (78) into Eq. (31), we find Eq. (79) of motion:

$$[\boldsymbol{K}]z + [\boldsymbol{M}]\ddot{z} = 0, \tag{79}$$

where [$\boldsymbol{K}$] is the stiffness matrix of the element, and [$\boldsymbol{M}$] is the mass matrix, which are defined by:

$$[\boldsymbol{K}] = \int [\boldsymbol{B}]^{TK} E(z) [\boldsymbol{B}]^{K} \, dV + \int [\boldsymbol{B}]^{Tf_e} k_{f_e} [\boldsymbol{B}]^{f_e} \, dS, \tag{80}$$

$$[\boldsymbol{M}] = \int [\boldsymbol{B}]^{TM} \rho(z) [\boldsymbol{B}]^{M} \, dV. \tag{81}$$

With $[\boldsymbol{B}]^{K}$, $[\boldsymbol{B}]^{f_e}$ the operator matrix of internal forces and elastic force foundation respectively. $[\boldsymbol{B}]^{TK}$, $[\boldsymbol{B}]^{Tf_e}$ are the operator matrix transpose of internal forces and elastic force foundation respectively.

3 Numerical study

To investigate how the correction coefficient and the intrinsic properties of functionally graded materials (FGMs) influence the vibrational behavior of beams, a detailed parametric study was undertaken. The analysis focused on a nanobeam composed of a metal–ceramic FGM system, specifically aluminum oxide (Al_2O_3) combined with a metallic phase, and supported by an elastic foundation. This configuration was selected to capture the combined effects of material gradation and foundation stiffness on dynamic performance. Particular attention was given to the sensitivity of natural frequencies and mode shapes to variations in both the correction coefficient and the spatial distribution of material properties across the beam's thickness. The geometric and mechanical parameters employed in the study, summarized in Table 1 [19], were carefully chosen to ensure physical relevance at the nanoscale while enabling systematic exploration of design variables. Such an approach provides insight into optimizing FGM nanobeams for high-precision engineering and advanced structural applications.

Table 2 presents the first three natural frequencies (Modes 1, 2, and 3) for functionally graded material (FGM) beams with a geometric ratio of L/h = 10, as a function of the material gradation index (p), comparing the results of Wattanasakulpong and Ungbhakorn [8] with the present findings. The present results are in very close agreement with those of Wattanasakulpong and Ungbhakorn [8],

Table 1 Representative mechanical and geometrical properties used in the modelling were derived from the data reported in Drici et al. [19]

Properties	Unit	Ceramic: alumina	Metal: aluminum
E	GPa	380	70
ρ	kg/m^3	3980	2702
v	–	0.3	0.3

indicating a satisfactory correlation between the current method and Wattanasakulpong and Ungbhakorn's [8] approach. As the gradation index p increases from 0 to 5, the natural frequencies gradually decrease across all modes. This trend confirms that a higher p-value corresponds to a higher ceramic content in the material composition, leading to a reduction in overall stiffness and, consequently, lower vibration frequencies. It is also observed that the frequency reduction is more pronounced for Mode 3 than for Mode 1, highlighting that higher-order modes are more sensitive to changes in the material gradation.

Table 3 illustrates the analysis of the combined effect of the Winkler (K_w) and Pasternak (K_p) foundation parameters on the first two natural frequencies Ω_1 and Ω_2 for FGM beams with $p = 2$. The present results are compared with those of Avcar and Mohammed [21]. It should be noted that the present results agree well with those of Avcar and Mohammed [21], with slight differences attributable to numerical methods or modelling assumptions, which demonstrates the validity and accuracy of the approach developed. When ($K_w = 0, K_p = 0$), the frequencies are lowest in this case, as a foundation support does not reinforce the beam. When K_w and K_p increase (e.g., $K_w = 10000$), the frequencies Ω_1 and Ω_2 increase significantly, illustrating the role of foundations in increasing the stiffness of the system and limiting vibrations. Thus, the combined K_w–K_p effect of a foundation in both K_w and K_p (e.g., $K_w = 10000$, $K_p = 1$) leads to even higher frequencies, confirming the stabilizing influence of the two foundation stiffnesses.

Table 4 presents a comparison of transverse shear correction factors for different combinations of the ratio (E_t/E_b) (Young's modulus of the ceramic to that of the metal) and the gradation index (p). The values are compared with those obtained by Menaa et al. [27] and Nguyen et al. [28]. The analysis reveals that the shear factor decreases with increasing (p), which means a reduction in the contribution of transverse shear to the overall deformation. This trend is attributed to a more uniform distribution of mechanical properties in highly graded beams. Furthermore, for low (E_t/E_b) ratios, the factors are more sensitive to variations in (p), highlighting the importance of the distribution of the modulus of elasticity in weakly heterogeneous configurations. The proposed results are in good agreement with those in Nguyen et al. [28] and Zou et al. [29], reinforcing the relevance of the assumptions adopted in the model.

Table 5 illustrates how the natural frequencies of functionally graded porous beams (Types I, II, III) vary with shear correction factors (κ) and elastic foundation parameters (K_w, K_p). Increasing K_w or K_p consistently raises the frequencies, confirming that foundation stiffness enhances beam rigidity. Type I beams show slightly higher frequencies than Types II and III, while changes in κ have only minor effects. The highest frequencies occur when both K_w and K_p are at their maximum, whereas the lowest occur with no foundation support. Overall, foundation stiffness dominates the vibrational response, with beam type and κ acting as secondary influences.

Table 2 Comparison of the first three frequencies $\Omega = \omega L^2 / h\sqrt{\rho_b / E_b}$ for FGM beams based on the p index ($L/h = 10$)

	Mode	Al_2O_3	$p = 0.2$	$p = 0.5$	$p = 1$	$p = 2$	$p = 5$
Wattanasakulpong and Ungbhakorn [8]	1	5.483	5.102	4.669	4.221	3.852	3.668
Present		5.463	5.116	4.790	4.504	4.271	4.001
Wattanasakulpong and Ungbhakorn [8]	2	21.933	20.408	18.676	16.884	15.407	14.670
Present		21.707	20.206	18.493	16.710	15.165	14.406
Wattanasakulpong and Ungbhakorn [8]	3	49.350	45.917	42.021	37.989	34.667	33.007
Present		48.821	45.590	41.874	38.018	34.190	32.354

Table 3 Comparison of the first two frequencies for FGM beams $p = 2$ as a function of foundation parameters K_w and K_p for ($L/h = 10$)

	K_w	K_p	Ω_1	Ω_2
Avcar and Mohammed [21]	0	0	3.852	15.407
Present			4.193	14.363
Avcar and Mohammed [21]	10000	0	27.133	30.964
Present			27.081	29.724
Avcar and Mohammed [21]	10000	0.5	27.198	31.190
Present			27.143	29.922
Avcar and Mohammed [21]	10000	1	27.262	31.415
Present			27.205	30.120

Table 4 Comparison of shear correction factors for FGM beams based on the E_t/E_b ratio and the p index for (L/h = 10)

p	E_t/E_b	Menaa et al. [27]	Nguyen et al. [28]	Present
0.2	2	0.8396	0.8396	0.8396
	4	0.8429	0.8429	0.8429
	6	0.8439	0.8440	0.8440
0.4	2	0.8411	0.8411	0.8411
	4	0.8453	0.8453	0.8453
	6	0.8467	0.8467	0.8467
2	2	0.8095	0.8095	0.8095
	4	0.7804	0.7804	0.7804
	6	0.7662	0.7662	0.7662
4	2	0.7905	0.7905	0.7905
	4	0.7247	0.7248	0.7247
	6	0.6784	0.6786	0.6784
6	2	0.7899	0.7899	0.7899
	4	0.7164	0.7163	0.7164
	6	0.6595	0.6595	0.6595

Table 5 Comparison of non-dimensional frequencies with different porosity distributions as a function of K_w and K_p for ratio E_t/E_b = 10 and index p = 5 for (L/h = 5) with $\left(\Omega = \omega L^2\sqrt{A/I \times \rho_t/E_t}\right)$

K_w	K_p	Type I		Type II		Type III	
		κ = 5/6	κ = 0.5501	κ = 5/6	κ = 0.5675	κ = 5/6	κ = 0.6017
0	0	6.2366	6.0699	6.2014	6.0544	5.9597	5.8418
	5	10.2640	9.9986	10.2504	10.0149	10.1367	9.9439
	10	13.1242	12.7974	13.1173	12.8263	13.0569	12.8190
50	0	10.6926	10.6068	10.6650	10.5891	10.5676	10.5094
	5	13.4554	13.2682	13.4384	13.2716	13.3860	13.2516
	10	15.7542	15.5002	15.7421	15.5148	15.7222	15.5387
100	0	13.7750	13.7164	13.7480	13.6960	13.7044	13.6653
	5	16.0227	15.8776	16.0030	15.8730	15.9875	15.8841
	10	18.0037	17.7968	17.9875	17.8014	17.9966	17.8481

Fig. 5 illustrates the variation in the shear correction factor k as a function of the gradient index p for a functional gradient material (FGM) with three porosity distributions (Types I, II, and III), each analyzed for three initial porosity levels: e_0 = 0, 0.1, and 0.2.

In all three cases, when the gradient index (p) varies from 0.5 to 1, the ceramic phase becomes dominant over the metallic phase, resulting in a material that is almost isotropic. Consequently, the shear correction factor (k) approaches an approximately constant value, close to that of a prismatic isotropic beam (k = 5/6), exhibiting a nonlinear variation in this range.

For gradient index values between 1 and 6, the material exhibits a heterogeneous structure (FGM), which requires an appropriate adjustment of the shear correction factor. As p further increases from 6 to 10, k shows a linear stabilization, indicating that the metallic phase becomes predominant in this region.

As an illustration, for the Type I porosity distribution, the shear correction factor (k) decreases by approximately 2% for an initial porosity of e_0 = 0.1 and by 4.5% for e_0 = 0.2. In the case of the Type II distribution, the variation of k is more moderate, with reductions of about 0.7% for e_0 = 0.1 and 1.8% for e_0 = 0.2.

Meaning that the Type III porosity distribution has no significant impact on the shear correction factor. These results demonstrate that the spatial distribution of porosity in an FGM plays an important role in the shear behavior of structures: for Type I distributions, the porous microstructure accentuates the dependence of k on initial porosity, whereas for Type III, this dependence is virtually non-existent. Furthermore, the convergence of k values for p > 5 in all three types indicates that in a predominantly metallic zone (high p), the effect of porosity and its distribution becomes negligible.

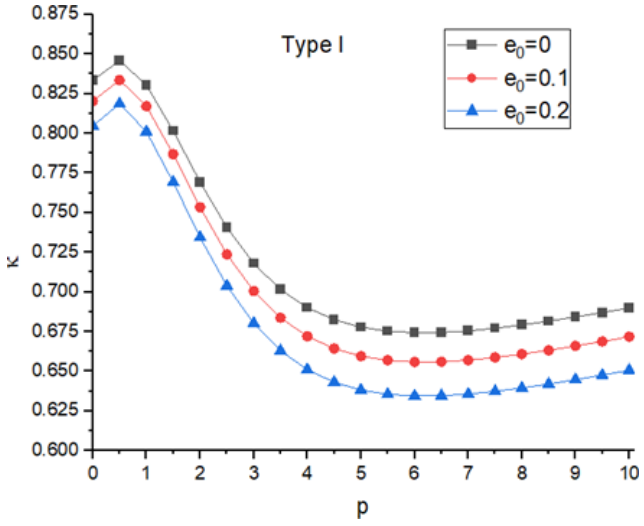

(a)

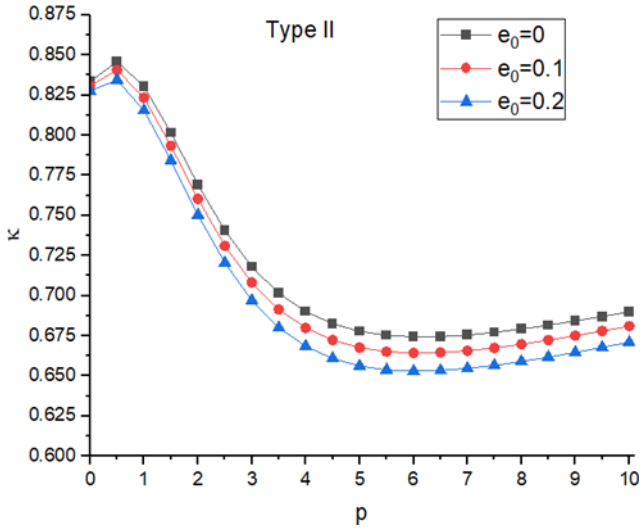

(b)

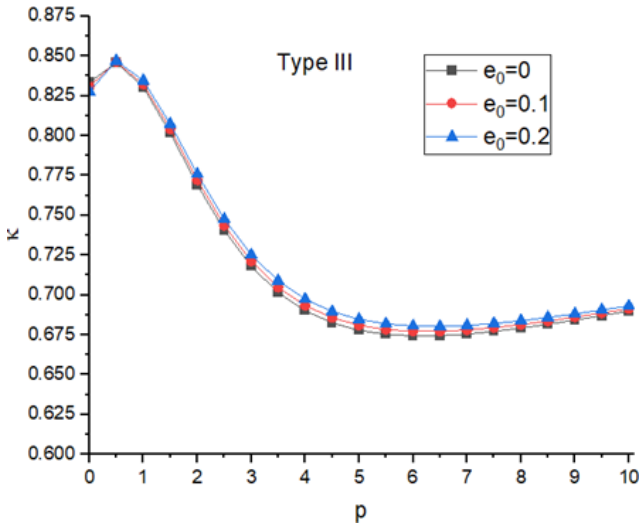

(c)

Fig. 5 Variation of the shear correction factor k for the three types of porosity (Type I, II and III) as a function of the FGM index p and different porosity parameters e_0: (a) center enhanced; (b) top enhanced; (c) bottom enhanced

Fig. 6 is plotted for different ratios of Young's moduli (E_t/E_b), where E_t represents the Young's modulus of the upper (ceramic) layer, and E_b corresponds to that of the lower (metallic) layer. When $E_t/E_b = 1$, the material behaves as an isotropic medium with a uniform Young's modulus $E = E_b$. In this case, the shear correction factor $k = 5/6$ remains constant for all values of p, confirming the absence of a gradient effect. Hence, the shear behavior does not depend on the position through the thickness, corresponding to an isotropic homogeneous beam.

When the ratio E_t/E_b increases (for example, 5, 10, 15, and 20), the material becomes heterogeneous, exhibiting a gradual transition between the ceramic phase (top) and the metallic phase (bottom). It can be observed that the shear correction factor k decreases significantly as p increases, indicating that the shear stiffness decreases under the combined influence of the material gradient and porosity. This behavior reflects a reduction in the effective contribution of the rigid ceramic layer as the metallic phase becomes dominant for high values of p:

- For $p \approx 0$–1: the material behaves as an isotropic ceramic, with a Young's modulus close to E_t. The value of k is relatively high, indicating a greater shear stiffness.
- For $1 < p < 6$: the material behaves as a functionally graded material (FGM), showing a progressive transition between the two phases. In this range, k decreases sharply, since the gradient in mechanical properties enhances shear flexibility. This region is therefore the most sensitive to variations in E_t/E_b and porosity distribution.
- For $p > 6$: the material becomes almost metallic, characterized by lower stiffness. The shear correction factor k tends toward a stable asymptotic value, indicating a stabilization of shear stiffness dominated by the metallic phase.
- Type I (porosity concentrated in the mid-plane): the factor k decreases gradually with increasing p. The symmetric distribution of porosity results in a smooth transition between phases and a moderate influence on shear behavior. The stabilization of k for $p > 5$ indicates that the metallic phase predominates without causing excessive loss of stiffness.
- Type II (porosity concentrated in the lower region): the decrease in k is faster, especially for higher E_t/E_b ratios. The concentration of porosity in the metallic zone, which is already more deformable, amplifies the loss of shear stiffness.

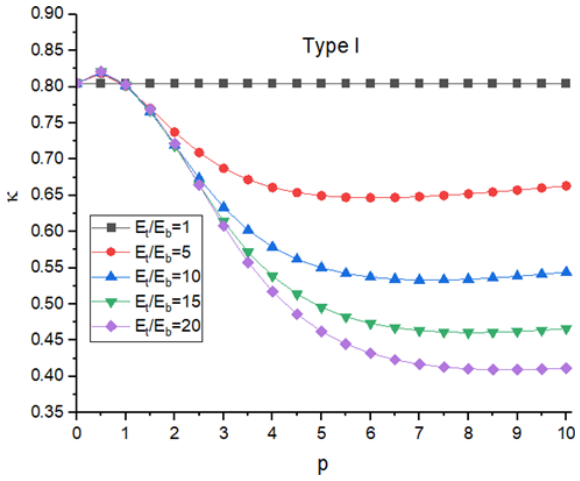

(a)

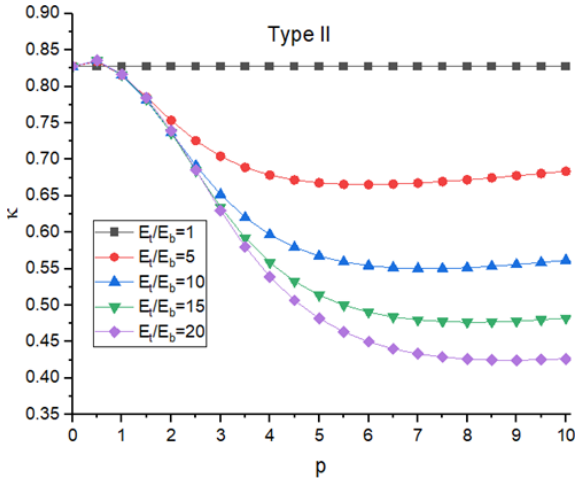

(b)

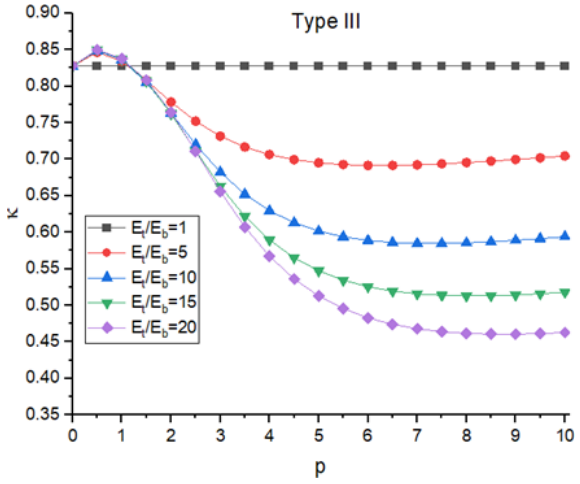

(c)

Fig. 6 Variation of the shear correction factor k for the three types of porosity (Type I, II and III) and material ratio E_t/E_b as a function of the FGM index p for a porosity $e_0 = 0.2$: (a) center enhanced; (b) top enhanced; (c) bottom enhanced

- Type III (porosity concentrated in the upper region): the factor k drops more sharply for $p > 2$. In this case, the porosity affects the rigid ceramic layer, leading to a significant reduction in overall stiffness. This behavior reveals a synergistic effect between the porosity distribution and the material gradient, resulting in a considerable decrease in shear resistance.

Fig. 7 illustrates the variation of non-dimensional natural frequencies (ω^*) of functionally graded porous beams with respect to the material gradient index p, considering different porosity distributions and shear correction factors (κ = 5/6 and corrected values). Across all three graphs, the results show a consistent decline in frequency as p increases, indicating that a higher material gradient index reduces structural stiffness and, consequently, the beam's resistance to vibration. This trend is more pronounced at low values of p (between 0 and 2), where frequencies decrease sharply, before gradually stabilizing for higher p values. The comparison between κ = 5/6 and corrected shear coefficients reveals that accounting for a refined shear correction factor slightly lowers the natural frequencies, reflecting the increased flexibility introduced by a more accurate representation of shear deformation. The differences, however, remain moderate, confirming that the shear correction factor plays a secondary role compared to the dominant influence of material gradation.

Moreover, the three porosity distributions demonstrate similar qualitative behavior, with only minor quantitative deviations in the frequency response. This suggests that although the manner in which porosity is distributed affects the vibrational performance, its impact is less significant than the combined effects of the material gradient index and the shear correction factor.

Overall, the Fig. 7 confirm that increasing p weakens the beam, reducing its natural frequencies. At the same time, the choice of porosity distribution and refinement of κ provides only secondary adjustments to the dynamic response.

4 Conclusions

The free vibration behavior of porous beams composed of functional gradient materials (FGM) supported by a Winkler-Pasternak elastic foundation and simulated using Timoshenko's theory is thoroughly examined in this paper. Such beams are widely employed in practical engineering applications, including aerospace structures, micro-electro-mechanical systems (MEMS), and civil engineering components, where effective vibration control and structural weight efficiency are of paramount importance. The principal advantage of the proposed methodology resides in its capability to accurately capture the coupled effects of porosity and material gradation on

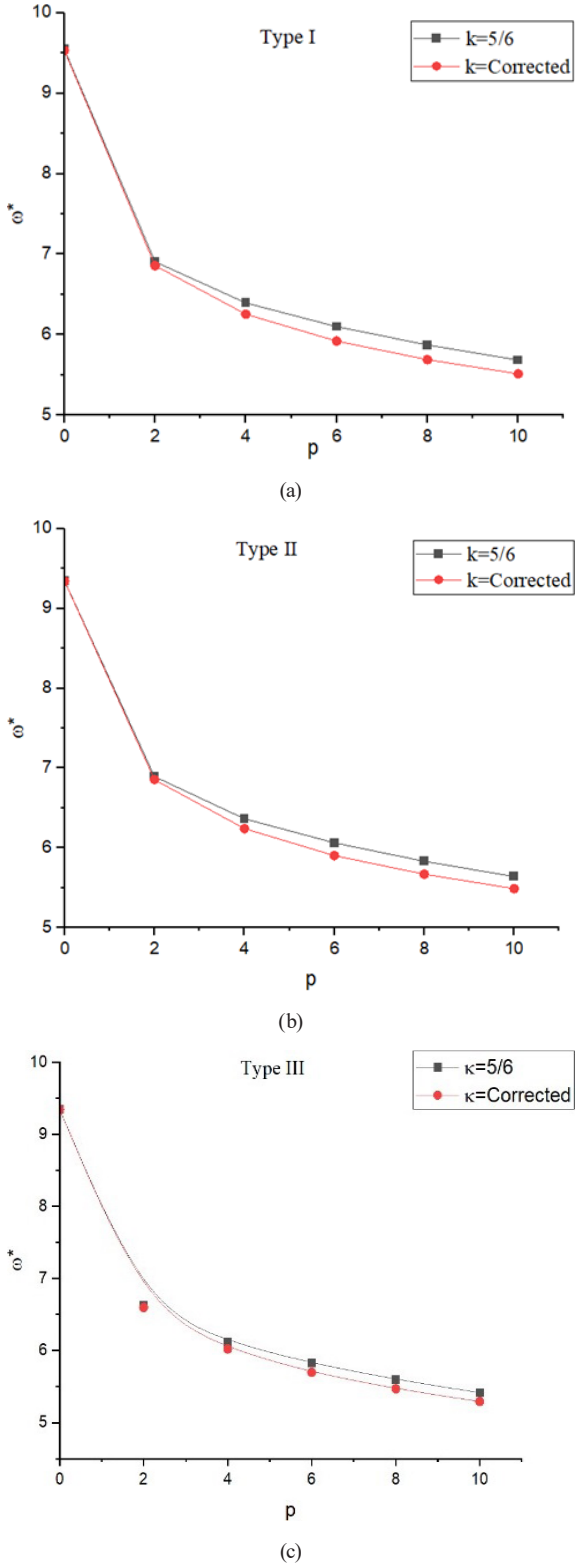

Fig. 7 Comparison of non-dimensional frequencies $\omega^* = \omega L^2 \sqrt{A/I \times \rho_c / E_c}$ with different porosity distributions as a function of p for ratio rapport ($E_t/E_b = 10$, $L/h = 5$, $K_w = 40$, $K_p = 10$): (a) center enhanced; (b) top enhanced; (c) bottom enhanced

transverse shear behavior, which are not adequately represented in conventional models employing constant shear correction factors. Moreover, the formulation exhibits a high degree of generality, allowing its application to a broad range of boundary conditions, material configurations, and elastic foundation parameters. The material gradation index p, foundation stiffnesses K_p and K_w, porosity distributions (Types I, II, and III), and the effects of transverse shear, which are simulated using an adjusted correction factor k, are among the important parameters that are examined in this work. Results from Wattanasakulpong and Ungbhakorn [8], Avcar and Mohammed [21], Menaa et al. [27] and Nguyen et al. [28] are compared with the model's validity. The study's findings offer a comprehensive and precise picture of the vibrational behavior of porous beams composed of functionally graded materials supported by elastic foundations. It is possible to reach the following conclusions:

- The proposed model is first validated by comparison with results available in Wattanasakulpong and Ungbhakorn [8], Avcar and Mohammed [21], Menaa et al. [27] and Nguyen et al. [28]. The results show excellent agreement, confirming the accuracy and reliability of the numerical approach adopted.
- The transverse shear correction factor shows that it is strongly influenced by the gradation index, the ratio (E_t/E_b), as well as by the distribution and level of porosity.
- The k factor decreases with increasing p, especially in the case of Type II and III porosity, reflecting a reduction in shear stiffness. This trend is accentuated when the modulus of the ceramic phase is significantly higher than that of the metallic phase. The role of porosity distribution is particularly significant: Type I is the most sensitive to variations in porosity, while Type III shows remarkable stability.
- The comparison between $\kappa = 5/6$ and corrected shear coefficients reveals that accounting for a refined shear correction factor slightly lowers the natural frequencies, reflecting the increased flexibility introduced by a more accurate representation of shear deformation. The differences, however, remain moderate, confirming that the shear correction factor plays a secondary role compared to the dominant influence of material gradation.

The overall system response is directly influenced by two critical factors:

1. the incorporation of the shear correction coefficient;
2. the effect of material property variations induced by porosity.

The chosen anisotropy modelling approach constitutes the fundamental element of this study for characterizing these materials. Indeed, the application of this specific correction is essential to prevent an overestimation of stiffness that would result from using a conventional factor. Consequently, it enables the establishment of enhanced and more realistic safety margins for the design of structures.

References

[1] Boumezbeur, K., Khebizi, M., Guenfoud, M., Guendouz, I. "Mechanical Response of Thin Composite Beams Made of Functionally Graded Material Using Finite Element Method", Periodica Polytechnica Civil Engineering, 67(4), pp. 970–982, 2023. https://doi.org/10.3311/PPci.21909

[2] Benyamina, A. B., Bouderba, B., Saoula, A. "Bending Response of Composite Material Plates with Specific Properties, Case of a Typical FGM "Ceramic/Metal" in Thermal Environments", Periodica Polytechnica Civil Engineering, 62(4), pp. 930–938, 2018. https://doi.org/10.3311/PPci.11891

[3] Souad, H., Ismail, M., Hichem, A., Noureddine, E. "Vibration Analysis of Viscoelastic FGM Nanoscale Plate Resting on Viscoelastic Medium Using Higher-order Theory", Periodica Polytechnica Civil Engineering, 65(1), pp. 255–275, 2021. https://doi.org/10.3311/PPci.16010

[4] Elmeiche, N., Abbad, H., Mechab, I., Bernard, F. "Free vibration analysis of functionally graded beams with variable cross-section by the differential quadrature method based on the nonlocal theory", Structural Engineering and Mechanics, 75(6), pp. 737–746, 2020. https://doi.org/10.12989/sem.2020.75.6.737

[5] Dadouch, M., Mechab, I., Elmeiche, N., Mechab, B. "New Investigation of the Buckling Responses of Nano-Beams Based on Engesser and Haringx Theories by the New Model of Shear Deformation Theories", Mechanics of Solids, 59(5), pp. 2992–3007, 2024. https://doi.org/10.1134/S0025654424604956

[6] Hamzi, S., Ghali, D., Mechab, I., Mechab, B., Elmeiche, N. "Quasi-3D Shear Deformation Theory for the Vibration Study of Viscoelastic FGM Nanoplates Resting on Visco Winkler–Pasternak Substrate Medium", Mechanics of Solids, 59(5), pp. 3108–3127, 2024. https://doi.org/10.1134/S0025654424604968

[7] Yu, W., Zhou, L. "Dynamic/static stability characteristics of sandwich FG porous beams", Steel and Composite Structures, 46(2), pp. 203–210, 2023. https://doi.org/10.12989/scs.2023.46.2.203

[8] Wattanasakulpong, N., Ungbhakorn, V. "Linear and nonlinear vibration analysis of elastically restrained ends FGM beams with porosities", Aerospace Science and Technology, 32(1), pp. 111–120, 2014. https://doi.org/10.1016/j.ast.2013.12.002

[9] Chen, D., Kitipornchai, S., Yang, J. "Nonlinear free vibration of shear deformable sandwich beam with a functionally graded porous core", Thin-Walled Structures, 107, pp. 39–48, 2016. https://doi.org/10.1016/j.tws.2016.05.025

[10] Wang, Y. Q., Zhao, H. L., Ye, C., Zu, J. W. "A Porous Microbeam Model for Bending and Vibration Analysis Based on the Sinusoidal Beam Theory and Modified Strain Gradient Theory", International Journal of Applied Mechanics, 10(05), 1850059, 2018. https://doi.org/10.1142/s175882511850059x

[11] Chen, D., Yang, J., Kitipornchai, S. "Elastic buckling and static bending of shear deformable functionally graded porous beam", Composite Structures, 133, pp. 54–61, 2015. https://doi.org/10.1016/j.compstruct.2015.07.052

[12] Sah, S. K., Ghosh, A. "Influence of porosity distribution on free vibration and buckling analysis of multi-directional functionally graded sandwich plates", Composite Structures, 279, 114795, 2022. https://doi.org/10.1016/j.compstruct.2021.114795

[13] Ebrahimi, F., Barati, M. R. "A general higher-order nonlocal couple stress based beam model for vibration analysis of porous nanocrystalline nanobeams", Superlattices and Microstructures, 112, pp. 64–78, 2017. https://doi.org/10.1016/j.spmi.2017.09.010

[14] Chinh, T. H., Tu, T. M., Duc, D. M., Hung, T. Q. "Static flexural analysis of sandwich beam with functionally graded face sheets and porous core via point interpolation meshfree method based on polynomial basic function", Archive of Applied Mechanics, 91(3), pp. 933–947, 2021. https://doi.org/10.1007/s00419-020-01797-x

[15] Akbaş, Ş. D. "Thermal Effects on the Vibration of Functionally Graded Deep Beams with Porosity", International Journal of Applied Mechanics, 9(5), 1750076, 2017. https://doi.org/10.1142/S1758825117500764

[16] Winkler, E. "Die Lehre von der Elasticitaet und Festigkeit" (The Theory of Elasticity and Strength), Dominicus, Prague, Czech Republic, 1867. (in German)

[17] Pasternak, P. L. "О новом методе расчета упругого основания при помощи двух коэффициентов постели" (On a New Method of Analysis of an Elastic Foundation by Means of Two Foundation Constants), Cosudarstrennoe Izdatelstvo Literatury po Stroitelstvui Arkhitekture, Moscow, Russia, 1954. (in Russian)

[18] Zhang, P., Schiavone, P., Qing, H. "Stress-driven local/nonlocal mixture model for buckling and free vibration of FG sandwich Timoshenko beams resting on a nonlocal elastic foundation", Composite Structures, 289, 115473, 2022. https://doi.org/10.1016/j.compstruct.2022.115473

[19] Drici, G., Mechab, I., Abbad, H., Elmeiche, N., Mechab, B. "Investigating the free vibration of viscoelastic FGM Timoshenko nanobeams resting on viscoelastic foundations with the shear correction factor using finite element method", Mechanics Based Design of Structures and Machines, 52(3), pp. 1278–1303, 2024. https://doi.org/10.1080/15397734.2022.2141777

[20] Nguyen Thi, H. "On mechanical behavior of two-layer functionally graded sandwich curved beams resting on elastic foundations using an analytical solution and refined Timoshenko beam theory", Ain Shams Engineering Journal, 13(4), 101674, 2022. https://doi.org/10.1016/j.asej.2021.11.016

[21] Avcar, M., Mohammed, W. K. M. "Free vibration of functionally graded beams resting on Winkler–Pasternak foundation", Arabian Journal of Geosciences, 11(10), 232, 2018.
https://doi.org/10.1007/s12517-018-3579-2

[22] Zenkour, A. M., Sobhy, M. "Nonlocal elasticity theory for thermal buckling of nanoplates lying on Winkler–Pasternak elastic substrate medium", Physica E: Low-Dimensional Systems and Nanostructures, 53, pp. 251–259, 2013.
https://doi.org/10.1016/j.physe.2013.04.022

[23] Tran, T. T., Tran, V. K., Pham, Q.-H., Zenkour, A. M. "Extended four-unknown higher-order shear deformation nonlocal theory for bending, buckling and free vibration of functionally graded porous nanoshell resting on elastic foundation", Composite Structures, 264, 113737, 2021.
https://doi.org/10.1016/j.compstruct.2021.113737

[24] Mohamed, I., Kahya, V., Şimşek, S. "A New Higher-Order Finite Element Model for Free Vibration and Buckling of Functionally Graded Sandwich Beams with Porous Core Resting on a Two-Parameter Elastic Foundation Using Quasi-3D Theory", Iranian Journal of Science and Technology, Transactions of Civil Engineering, 49(1), pp. 383–408, 2025.
https://doi.org/10.1007/s40996-024-01482-x

[25] Nguyen, N.-D., Nguyen, T.-N., Nguyen, T.-K., Vo, T. P. "A Legendre-Ritz solution for bending, buckling and free vibration behaviours of porous beams resting on the elastic foundation", Structures, 50, pp. 1934–1950, 2023.
https://doi.org/10.1016/j.istruc.2023.03.018

[26] Marinetti, A. "On the Accuracy of Shear Factors for Elastic Uniform Beams: Evaluation Using the Boundary Element Method", In: Badalà, A., Marinetti, A., Motta, F., Oliveto, F. (eds.) Materiali e Metodi Innovativi Nell'Ingegneria Strutturale: Convegno in onore di Antonio La Tegola, Aracne Editrice, 2009, pp. 291–318. ISBN 8854824518
https://doi.org/10.4399/978885482451519

[27] Menaa, R., Tounsi, A., Mouaici, F., Mechab, I., Zidi, M., Bedia, E. A. A. "Analytical Solutions for Static Shear Correction Factor of Functionally Graded Rectangular Beams", Mechanics of Advanced Materials and Structures, 19(8), pp. 641–652, 2012.
https://doi.org/10.1080/15376494.2011.581409

[28] Nguyen, T.-K., Sab, K., Bonnet, G. "First-order shear deformation plate models for functionally graded materials", Composite Structures, 83(1), pp. 25–36, 2008.
https://doi.org/10.1016/j.compstruct.2007.03.004

[29] Zou, D., Liu, G., Rao, Z., Tan, T., Zhang, W., Liao, W.-H. "A device capable of customizing nonlinear forces for vibration energy harvesting, vibration isolation, and nonlinear energy sink", Mechanical Systems and Signal Processing, 147, 107101, 2021.
https://doi.org/10.1016/j.ymssp.2020.107101

[30] Zhang, P., Wang, Z., Tian, H., Xi, X., Liu, X. "On the Magnetically Tunable Free Damped-Vibration of L-Shaped Composite Spherical Panels Made of GPL-Reinforced Magnetorheological Elastomers: An Element-Based GDQ Approach", Thin-Walled Structures, 218, 113987, 2026.
https://doi.org/10.1016/j.tws.2025.113987

[31] Tang, C., Lu, Z., Qin, L., Yan, T., Li, J., Zhao, Y., Qiu, Y. "Coupled vibratory roller and layered unsaturated subgrade model for intelligent compaction", Computers and Geotechnics, 177, 106827, 2025.
https://doi.org/10.1016/j.compgeo.2024.106827

[32] Deng, J., Gao, N. "Broadband vibroacoustic reduction for a circular beam coupled with a curved acoustic black hole via null-space method", International Journal of Mechanical Sciences, 233, 107641, 2022.
https://doi.org/10.1016/j.ijmecsci.2022.107641

[33] Wei, J., Xie, Z., Zhang, W., Luo, X., Yang, Y., Chen, B. "Experimental study on circular steel tube-confined reinforced UHPC columns under axial loading", Engineering Structures, 230, 111599, 2021.
https://doi.org/10.1016/j.engstruct.2020.111599

[34] Dai, J., Yang, C., Gai, P.-P., Xu, Z.-D., Yan, X., Xu, W.-P. "Robust damping improvement against the vortex-induced vibration in flexible bridges using multiple tuned mass damper inerters", Engineering Structures, 313, 118221, 2024.
https://doi.org/10.1016/j.engstruct.2024.118221

[35] Zhou, X., Lu, D., Zhao, J., Zhang, Y., Gao, Z., Rabczuk, T., Du, X. "Material characteristic length insensitive nonlocal modelling: A computationally efficient scaled nonlocal integral method", Computers and Geotechnics, 188, 107587, 2025.
https://doi.org/10.1016/j.compgeo.2025.107587

[36] Long, X., Iyela, P. M., Su, Y., Atlaw, M. M., Kang, S.-B. "Numerical predictions of progressive collapse in reinforced concrete beam-column sub-assemblages: A focus on 3D multiscale modeling", Engineering Structures, 315, 118485, 2024.
https://doi.org/10.1016/j.engstruct.2024.118485

[37] Ma, C., Zheng, H., Yang, N., Sun, T., Si, J., Ren, D. "Microstructural evolution and mechanical properties of snow under compression", Construction and Building Materials, 472, 140883, 2025.
https://doi.org/10.1016/j.conbuildmat.2025.140883

[38] Lu, D., Meng, F., Zhou, X., Zhuo, Y., Gao, Z., Du, X. "A Dynamic Elastoplastic Model of Concrete Based on a Modeling Method with Environmental Factors as Constitutive Variables", Journal of Engineering Mechanics, 149(12), 04023102, 2023.
https://doi.org/10.1061/JENMDT.EMENG-7206

[39] Dhuria, M., Grover, N., Goyal, K. "Influence of porosity distribution on static and buckling responses of porous functionally graded plates", Structures, 34, pp. 1458–1474, 2021.
https://doi.org/10.1016/j.istruc.2021.08.050

[40] Srikarun, B., Songsuwan, W., Wattanasakulpong, N. "Linear and nonlinear static bending of sandwich beams with functionally graded porous core under different distributed loads", Composite Structures, 276, 114538, 2021.
https://doi.org/10.1016/j.compstruct.2021.114538

[41] Tran, T. T., Pham, Q.-H., Nguyen-Thoi, T. "Static and free vibration analyses of functionally graded porous variable-thickness plates using an edge-based smoothed finite element method", Defence Technology, 17(3), pp. 971–986, 2021.
https://doi.org/10.1016/j.dt.2020.06.001

[42] Kiarasi, F., Babaei, M., Sarvi, P., Asemi, K., Hosseini, M., Omidi Bidgoli, M. "A review on functionally graded porous structures reinforced by graphene platelets", Journal of Computational Applied Mechanics, 52(4), pp. 731–750, 2021.
https://doi.org/10.22059/jcamech.2021.335739.675